

Surface motion of multiple alluvial valleys for incident plane SH-waves by using a semi-analytical approach

Jeng-Tzong Chen^{*}, Po-Yuan Chen, Chia-Tsung Chen

Department of Harbor and River Engineering, National Taiwan Ocean University, Keelung, Taiwan

Received 7 August 2006; received in revised form 31 March 2007; accepted 2 April 2007

Abstract

In this paper, the degenerate kernels and Fourier series expansions are adopted in the null-field integral equation to solve the exterior Helmholtz problems with alluvial valleys. The main gain of using degenerate kernels in integral equations is free of calculating the principal values for singular integrals by locating the null-field point exactly on the real boundary. An adaptive observer system is addressed to fully employ the property of degenerate kernels for circular boundaries in the polar coordinate. Image concept and technique of decomposition are utilized for half-plane problems. After moving the null-field point to the real boundary and matching the boundary conditions, a linear algebraic system is obtained without boundary discretization. The unknown coefficients in the algebraic system can be easily determined. The present method is treated as a “semi-analytical” solution since error only attributes to the truncation of Fourier series. Earthquake analysis for the site response of alluvial valley or canyon subject to the incident SH-wave is the main concern. Numerical examples including single and successive alluvial valleys are given to test our program. Limiting cases of a single canyon and two successive canyons are also addressed. Amplification of soft basin is also observed in this study. The validity of the semi-analytical method is verified. Our advantages, well-posed model, principal value free, elimination of boundary-layer effect and exponential convergence and mesh-free, by using the present method are achieved.

© 2007 Elsevier Ltd. All rights reserved.

Keywords: Degenerate kernel; Fourier series; Null-field integral equation; Helmholtz problem; Alluvial valley

1. Introduction

One of the major concerns of engineering seismology is to understand and explain vibrational response of the soil excited by earthquakes. The problem of the scattering and diffraction of SH-waves by a two-dimensional arbitrary number and location of cavities and inclusions in full and half-planes is revisited in this paper by using our unified formulation. In 1971, Trifunac [1] has solved the problem of a single semi-circular alluvial valley subject to SH-wave. Later, Pao and Mow [2] have published a book on the stress concentration in 1972. In 1973, Trifunac [3] has also derived the closed-form solution of a single semi-circular canyon subject to the SH-wave. The earliest reference to a closed-form solution of the scattering and diffraction of the incident SH-wave by an underground inclusion exists in an

article concerning an underground circular tunnel by Lee and Trifunac [4]. In order to extend to arbitrary shape inclusion problems, Lee and Manoogian [5] have used the weighted residual method to revisit the problem of scattering and diffraction of SH-wave with respect to an underground cavity of arbitrary shape in a two-dimensional elastic half-plane. In the following years, they extended to the half-plane problem with an inclusion of arbitrary shape [6,7]. According to the literature review, it is observed that exact solutions for boundary value problems (BVPs) are only limited for simple cases, e.g. half-plane with a semi-circular canyon, a cavity under half-plane, an inclusion under half-plane. Numerical approach using boundary integral formulation was employed to study diffraction of seismic waves in half-plane [8]. Therefore, proposing a systematic approach for solving exterior Helmholtz problems with circular boundaries of various numbers, positions and radii is our goal in this paper.

^{*}Corresponding author. Tel: 886 2 24622192x6140; fax: 886 2 24632375.
E-mail address: jtchen@mail.ntou.edu.tw (J.-T. Chen).

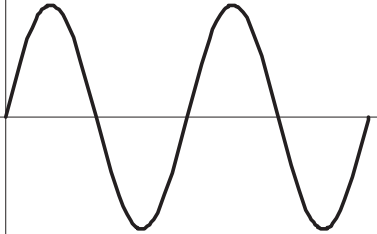
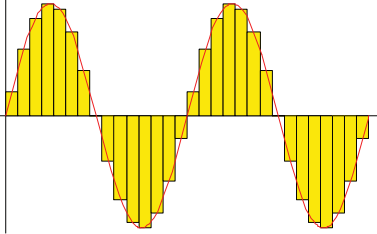
For a problem with several holes, various numerical methods, e.g. finite difference method (FDM), finite element method (FEM), boundary element method (BEM) and meshfree method, etc. are always resorted to solve. A much more general problem for SH-waves, the numerical solution of time-harmonic transition problems in elasticity, in general, and with soil amplification in inhomogeneous alluvial valleys, was obtained by using boundary element–finite element (BEM–FEM) [9] formulation. Among diverse numerical approaches, FEM and BEM have become popular research tools for engineers. In the past decade, FEM has been widely applied to carry out many engineering problems, but one disadvantage is that discretizations on the domain are time-consuming to set up the mesh models. Regarding to the benefit of using BEM, only discretizations on boundaries are required and the boundary conditions at infinity are automatically satisfied. Discrete wave number BEM [10–12] utilized discrete wave number approach to calculate Green's function in the BEM or boundary integral equation method (BIEM). Indirect BEM [13] employs only single-layer potential representation for the solution. However, the discrete wave number BEM determines Green's function using the sum of discrete wave number. Although BEM has been involved as an alternative method for solving engineering problems, four critical issues are of concern.

1. In the dual BIEM/BEM formulation, the singular and hypersingular integrals need special care on the sense of the Cauchy and Hadamard principal values, respectively. How to determine accurately the free terms has received more attentions in the past decade and a large amount of papers can be found. Two conventional approaches were employed to regularize the singular and hypersingular integrals. First, Guiggiani [14] has derived the free terms for Laplace and Navier equations using differential geometry and bump contour approach. Second, Gray and Manne [15] have employed a limiting process to ensure a finite value from an interior point to boundary by using symbolic software. Two alternatives, fictitious BEM and null-field approach (off boundary approach), can avoid the singularity since the source and field points never coincide in the boundary integration. However, they result in an ill-posed matrix which will be elaborated on later.
2. On the other hand, many researchers tried to regularize the approach to regular formulation. In order to avoid directly calculating the singular and hypersingular integrals, null-field approach [16,17] or fictitious BEM [18] yields an ill-conditioned system which needs regularization. In the paper, we may wonder whether it is possible to push the null-field point on the real boundary but free of calculating singularity and hypersingularity. The answer is yes. Instead of determining the singular (hypersingular) integrals using the definition of CPV (HPV), the kernel function is described in an analytical form from each side (interior and exterior) by employing the separable technique since the double-layer potential is discontinuous across the boundary. Therefore, degenerate kernel, namely separable kernel, is employed to represent the potential of the perforated domain which satisfies the governing equation.
3. Boundary-layer effect is inherent in BEM. In real applications, data near boundary can be artificially smoothed since Laplace field satisfies maximum and minimum principles. Nevertheless, it also deserves study to know how to manipulate the nearly singular integrals. We may wonder whether it is possible to develop a BIEM formulation which is free of boundary-layer effect. Readers can find the answer in this paper.
4. Convergence rate is the main concern of BEM. It is no doubt that dual BEM is very versatile for BVPs with general geometries including circular holes, ellipse, square and crack boundaries. Regarding to constant, linear and quadratic elements, the discretization scheme does not take the geometry into consideration. For problems with special geometries, one can propose the special function to approximate the geometry. Fourier series is specially tailored to problems with circular geometries. In the book of Kress and Atkinson [19,20], the degenerate kernel is defined that the source and field points in the fundamental solution can be separated. Kress also proved that expansion of degenerate kernel and Fourier series yields the exponential convergence instead of linear algebraic convergence using BEM. The numerical experiment was performed for Helmholtz problems in his paper [21]. This paper takes the advantage of this expansion to deal with problems containing circular boundary using Fourier series in conjunction with degenerate kernel.

A new approach to have the four gains: (1) principal value free, (2) well-posed, (3) elimination of boundary-layer effect and (4) exponential convergence, is the goal of this paper. Table 1 shows the comparisons of the present method and conventional BEM.

In this paper, the BIEM is utilized to solve the half-plane radiation and scattering problems with circular boundaries. To fully utilize the geometry of circular boundary after introducing image concept, not only Fourier series for boundary densities as previously used by many researchers but also the degenerate kernel for fundamental solutions in the present formulation is incorporated into the null-field integral equation. The key idea is that we can push the null-field point exactly on the real boundary by using appropriate degenerate kernel in real computation. All the improper boundary integrals are free of calculating the principal values (Cauchy and Hadamard) in place of series sum. In integrating each circular boundary for the null-field equation, the adaptive observer system of polar coordinate is considered to fully employ the property of degenerate kernel. For the hypersingular equation, vector decomposition for the radial and tangential gradients is

Table 1
Comparisons of the present method and conventional BEM

Boundary density discretization	Auxiliary system	Formulation	Observer system	Singularity
Present method Fourier series 	Degenerate kernel	Null-field integral equation	Adaptive observer system	No principal value
Conventional BEM Constant element 	Fundamental solution	Boundary integral equation	Fixed observer system	Principal value (CPV, RPV and HPV)

CPV, RPV and HPV are the Cauchy principal value, Riemann principal value and Hadamard principal value, respectively.

carefully considered, especially in the non-focal case. A scattering problem subject to the incident wave is decomposed into two parts, incident plane wave field and radiation field. The radiation boundary condition is the minus quantity of incident wave function for matching the boundary condition of total wave for a cavity. Not only a semi-analytical approach is proposed but also the amplification of site response for alluvial valleys is studied. Our approach can deal with a cavity problem as a limiting case of an inclusion problem with zero shear modulus.

2. Problem statement

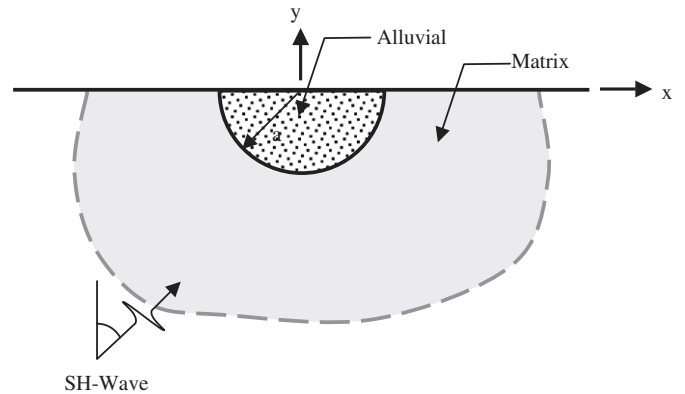
Half-plane problems with alluvial to be analyzed is shown in Fig. 1. The matrix and alluvial are assumed to be elastic, isotropic and homogenous, and the interface between the alluvial and matrix is assumed to be perfect. The governing equation of the anti-plane SH-wave harmonic motion is

$$\mu \nabla^2 w(x) + \rho \omega^2 w(x) = 0, \quad x \in \Omega, \tag{1}$$

where μ , ρ and ω are the material properties of shear modulus, the density and the frequency, ∇^2 and Ω are the Laplacian operator and the domain of interest, respectively. The anti-plane displacement field is defined as

$$u = v = 0, \quad w = w(x, y), \tag{2}$$

where w is the only non-vanishing component of displacement with respect to the Cartesian coordinate which is a function of x and y . The traction free boundary



- ρ_I : density of alluvial
- ρ_M : density of matrix
- μ_I : shear modulus of alluvial
- μ_M : shear modulus of matrix
- γ : the angle of incident wave and y-axis

Fig. 1. A half-plane problem with a semi-circular alluvial valley subject to the SH-wave.

condition at the ground surface of the half-plane is defined as follows:

$$\tau_{yz} = \mu \frac{\partial w}{\partial y} = 0, \quad y = 0, \tag{3}$$

or can be represented in the polar coordinate as

$$\tau_\theta = \frac{\mu}{r} \frac{\partial w}{\partial \theta} = 0, \quad \theta = 0 \text{ and } \pi. \quad (4)$$

The incident excitation of the half-plane, w^{in} , is defined as a steady-state plane SH-wave, and motion in the z direction. It is expressed as

$$w^{\text{in}} = W_0 e^{ik(x \sin \gamma + y \cos \gamma)}, \quad (5)$$

where W_0 is the constant amplitude, and γ is the angle of incidence.

3. Dual boundary integral equations and dual null-field integral equations

For the SH-wave problem, the integral equation for the domain point can be derived from the third Green's identity [22], yields

$$2\pi u(x) = \int_B T^e(s, x) u(s) dB(s) - \int_B U^e(s, x) t(s) dB(s), \quad x \in \Omega \cup B, \quad (6)$$

$$2\pi t(x) = \int_B M^e(s, x) u(s) dB(s) - \int_B L^e(s, x) t(s) dB(s), \quad x \in \Omega \cup B, \quad (7)$$

where the four kernels should be selected in a degenerate form of exterior region with the superscript “e”, s and x are the source and field points, respectively, B is the boundary, and the kernel function, $U(s, x)$, is the fundamental solution which satisfies

$$(\nabla^2 + k^2)U(x, s) = 2\pi\delta(x - s), \quad (8)$$

where $\delta(x-s)$ denotes the Dirac-delta function. Then, we can obtain the fundamental solution as follows:

$$U(s, x) = \frac{-i\pi H_0^{(1)}(kr)}{2}, \quad (9)$$

$$T(s, x) = \frac{\partial U(s, x)}{\partial n_s}, \quad L(s, x) = \frac{\partial U(s, x)}{\partial n_x}, \quad M(s, x) = \frac{\partial^2 U(s, x)}{\partial n_x \partial n_s}, \quad (10)$$

where $H_n^{(1)}(kr)$ is the n th-order Hankel function of the first kind, $r \equiv |s - x|$, n_x denotes the outward normal vector at the field point x . By collocating x outside the domain ($x \in \Omega^c$), we obtain the dual null-field integral equations as

$$0 = \int_B T^i(s, x) u(s) dB(s) - \int_B U^i(s, x) t(s) dB(s), \quad x \in \Omega^c \cup B, \quad (11)$$

$$0 = \int_B M^i(s, x) u(s) dB(s) - \int_B L^i(s, x) t(s) dB(s), \quad x \in \Omega^c \cup B, \quad (12)$$

where Ω^c is the complementary domain and the four kernels are chosen appropriately using degenerate expression of interior region with the superscript “i” in the following section.

4. Expansions of fundamental solution and boundary density

In the present method, we adopt the mathematical tools, degenerate kernels, for the purpose of analytical study. The combination of degenerate kernels and Fourier series plays the major role in handling problems with circular boundaries. Based on the separable property, the kernel function $U(s, x)$, $T(s, x)$, $L(s, x)$ and $M(s, x)$ can be expanded into separable form by separating the source point ($s = (R, \theta)$) and field point ($x = (\rho, \phi)$) in the polar coordinate [23].

$$U(s, x) = \begin{cases} U^i(s, x) = \frac{-\pi i}{2} \sum_{m=0}^{\infty} \varepsilon_m J_m(k\rho) H_m^{(1)}(kR) \cos(m(\theta - \phi)), & R \geq \rho, \\ U^e(s, x) = \frac{-\pi i}{2} \sum_{m=0}^{\infty} \varepsilon_m H_m^{(1)}(k\rho) J_m(kR) \cos(m(\theta - \phi)), & \rho > R, \end{cases} \quad (13)$$

$$T(s, x) = \begin{cases} T^i(s, x) = \frac{-\pi k i}{2} \sum_{m=0}^{\infty} \varepsilon_m J_m(k\rho) H_m^{(1)}(kR) \cos(m(\theta - \phi)), & R > \rho, \\ T^e(s, x) = \frac{-\pi k i}{2} \sum_{m=0}^{\infty} \varepsilon_m H_m^{(1)}(k\rho) J_m(kR) \cos(m(\theta - \phi)), & \rho > R, \end{cases} \quad (14)$$

$$L(s, x) = \begin{cases} L^i(s, x) = \frac{-\pi k i}{2} \sum_{m=0}^{\infty} \varepsilon_m J_m'(k\rho) H_m^{(1)}(kR) \cos(m(\theta - \phi)), & R > \rho, \\ L^e(s, x) = \frac{-\pi k i}{2} \sum_{m=0}^{\infty} \varepsilon_m H_m^{(1)}(k\rho) J_m'(kR) \cos(m(\theta - \phi)), & \rho > R, \end{cases} \quad (15)$$

$$M(s, x) = \begin{cases} M^i(s, x) = \frac{-\pi k^2 i}{2} \sum_{m=0}^{\infty} \varepsilon_m J_m'(k\rho) H_m^{(1)}(kR) \cos(m(\theta - \phi)), & R \geq \rho, \\ M^e(s, x) = \frac{-\pi k^2 i}{2} \sum_{m=0}^{\infty} \varepsilon_m H_m^{(1)}(k\rho) J_m'(kR) \cos(m(\theta - \phi)), & \rho > R, \end{cases} \quad (16)$$

where $i^2 = -1$ the superscripts “i” and “e” denote the interior and exterior cases for the expressions of kernel, respectively, and ε_m is the Neumann factor

$$\varepsilon_m = \begin{cases} 1, & m = 0, \\ 2, & m = 1, 2, \dots, \infty. \end{cases} \quad (17)$$

It is noted that the larger argument is imbedded in the complex Hankel function (H) instead of real Bessel function (J) to ensure the $H_0(kr)$ singularity and series convergence. Since the potential resulted from $T(s, x)$ and $L(s, x)$ kernels are discontinuous across the boundary, the potentials of $T(s, x)$ for $R \rightarrow \rho^+$ and $R \rightarrow \rho^-$ are different.

This is the reason why $R = \rho$ is not included in expressional degenerate kernels of $T(s, x)$ and $L(s, x)$ in Eqs. (14) and (15). The analytical evaluation of the integrals for each element in the influence matrix is listed in the Appendix and they are all non-singular. Besides, the limiting case to the boundary is also addressed. The continuous and jump behavior across the boundary is well described by using the Wronskian property of J_m and Y_m

$$\begin{aligned} W(J_m(kR), Y_m(kR)) &= Y'_m(kR)J_m(kR) - Y_m(kR)J'_m(kR) \\ &= \frac{2}{\pi kR} \end{aligned} \quad (18)$$

to display the jump behavior as

$$\begin{aligned} &\int_0^{2\pi} (T^i(s, x) - T^e(s, x)) \cos(n\theta) R d\theta \\ &= kR\pi^2 J_n(kR) [Y'_n(kR) - iJ'_n(kR)] \cos(n\phi) \\ &\quad - kR\pi^2 J'_n(kR) [Y_n(kR) - iJ_n(kR)] \cos(n\phi) \\ &= 2\pi \cos(n\phi), \end{aligned} \quad (19)$$

$$\begin{aligned} &\int_0^{2\pi} (T^i(s, x) - T^e(s, x)) \sin(n\theta) R d\theta \\ &= kR\pi^2 J_n(kr) [Y'_n(kr) - iJ'_n(kR)] \sin(n\phi) \\ &\quad - kR\pi^2 J'_n(kr) [Y_n(kr) - iJ_n(kR)] \sin(n\phi) \\ &= 2\pi \sin(n\phi), \end{aligned} \quad (20)$$

where J and Y functions are similar to the Wronskian of two bases, 1 and x , for one-dimensional rod case.

Since only circular boundary is considered in this study, we employ the Fourier series expansions to approximate the potential u and its normal derivative t on the circular boundary, we have

$$\begin{aligned} u(s_k) &= a_0^k + \sum_{n=1}^{\infty} (a_n^k \cos n\theta_k + b_n^k \sin n\theta_k), \\ s_k &\in B_k, \quad k = 1, 2, \dots, N, \end{aligned} \quad (21)$$

$$\begin{aligned} t(s_k) &= p_0^k + \sum_{n=1}^{\infty} (p_n^k \cos n\theta_k + q_n^k \sin n\theta_k), \\ s_k &\in B_k, \quad k = 1, 2, \dots, N, \end{aligned} \quad (22)$$

where $t(s_k) = \partial u(s_k) / \partial n_s$ in which n_s denotes the outward normal vector at the source point s , a_n^k , b_n^k , p_n^k and q_n^k ($n = 0, 1, 2, \dots$) are the Fourier coefficients and θ_k is the polar angle for the k th circular boundary.

5. Adaptive observer system

Consider a BVP with circular boundaries of arbitrary locations. The rule of objectivity is obeyed since the boundary integral equations are frame indifferent. An adaptive observer system is addressed to fully employ the property of degenerate kernels for circular boundaries in the polar coordinate as shown in Figs. 2(a) and (b). For the integration, the origin of the observer system can be

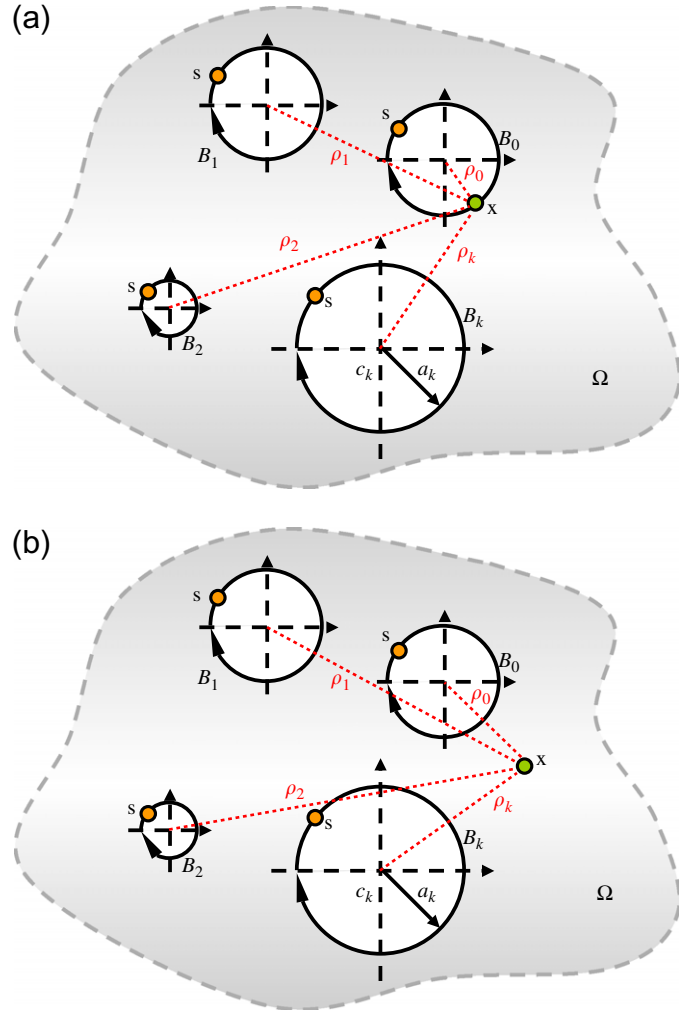


Fig. 2. (a) Sketch of the null-field integral equation in conjunction with the adaptive observer system. (b) Sketch of the boundary integral equation for the domain point in conjunction with the adaptive observer system.

adaptively located on the center of the corresponding boundary contour. The dummy variable in the circular boundary integration is the angle (θ) instead of radial coordinate (R). By using the adaptive system, all the integrations can be easy to calculate.

6. Linear algebraic system

In order to calculate the Fourier coefficients, $2L+1$ boundary nodes are needed. By locating the null-field point exactly on the j th circular boundary for Eq. (11) and (12), we have

$$\begin{aligned} 0 &= \sum_{j=1}^N \int_{B_j} T(s, x) u(s) dB(s) \\ &\quad - \sum_{j=1}^N \int_{B_j} U(s, x) t(s) dB(s), \quad x \in \Omega^e \cup B, \end{aligned} \quad (23)$$

$$0 = \sum_{j=1}^N \int_{B_j} M(s, x)u(s) dB(s) - \sum_{j=1}^N \int_{B_j} L(s, x)t(s) dB(s), \quad x \in \Omega^c \cup B. \quad (24)$$

It is noted that the integration path is anticlockwise for the outer circle. Otherwise, it is clockwise. For the B_j

integral of the circular boundary, the kernel of $U(s, x)$ is expressed in terms of degenerate kernel of Eq. (13), and $T(s, x)$, $L(s, x)$ and $M(s, x)$ are, respectively obtained by applying the differential operators defined in Eq. (10). The boundary densities $u(s)$ and $t(s)$ are substituted by using the Fourier series of Eqs. (21) and (22), respectively. In the B_j integration, we set the origin of the observer system to collocate at the center c_j to fully utilize the degenerate kernel and Fourier series. By moving the null-field point to B_j , a linear algebraic system is obtained

$$[\mathbf{U}]\{\mathbf{t}\} = [\mathbf{T}]\{\mathbf{u}\}, \quad (25)$$

where $[\mathbf{U}]$ and $[\mathbf{T}]$ are the influence matrices with a dimension of $N \times N$, $\{\mathbf{u}\}$ and $\{\mathbf{t}\}$ denote the column vectors of Fourier coefficients with a dimension of $N \times 1$ in which those can be defined as follows

$$[\mathbf{U}] = \begin{bmatrix} \mathbf{U}_{11} & \mathbf{U}_{12} & \cdots & \mathbf{U}_{1N} \\ \mathbf{U}_{21} & \mathbf{U}_{22} & \cdots & \mathbf{U}_{2N} \\ \vdots & \vdots & \ddots & \vdots \\ \mathbf{U}_{N1} & \mathbf{U}_{N2} & \cdots & \mathbf{U}_{NN} \end{bmatrix}, \quad [\mathbf{T}] = \begin{bmatrix} \mathbf{T}_{11} & \mathbf{T}_{12} & \cdots & \mathbf{T}_{1N} \\ \mathbf{T}_{21} & \mathbf{T}_{22} & \cdots & \mathbf{T}_{2N} \\ \vdots & \vdots & \ddots & \vdots \\ \mathbf{T}_{N1} & \mathbf{T}_{N2} & \cdots & \mathbf{T}_{NN} \end{bmatrix}, \quad (26)$$

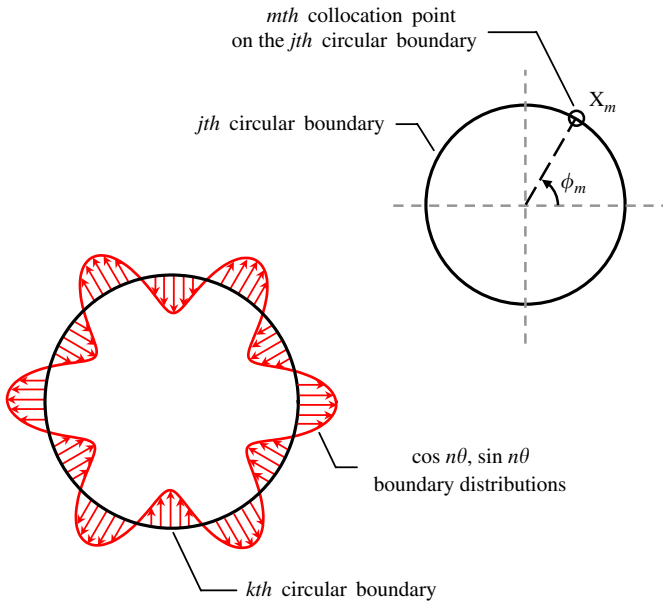


Fig. 3. Physical meaning of influence coefficients $U_{jk}^{mc}(\phi_m)$: $U_{jk}^{ns}(\phi_m)$: the responses for the x_m point of the j th boundary due to the $\cos n\theta$, $\sin n\theta$ boundary distributions of the k th circular boundary.

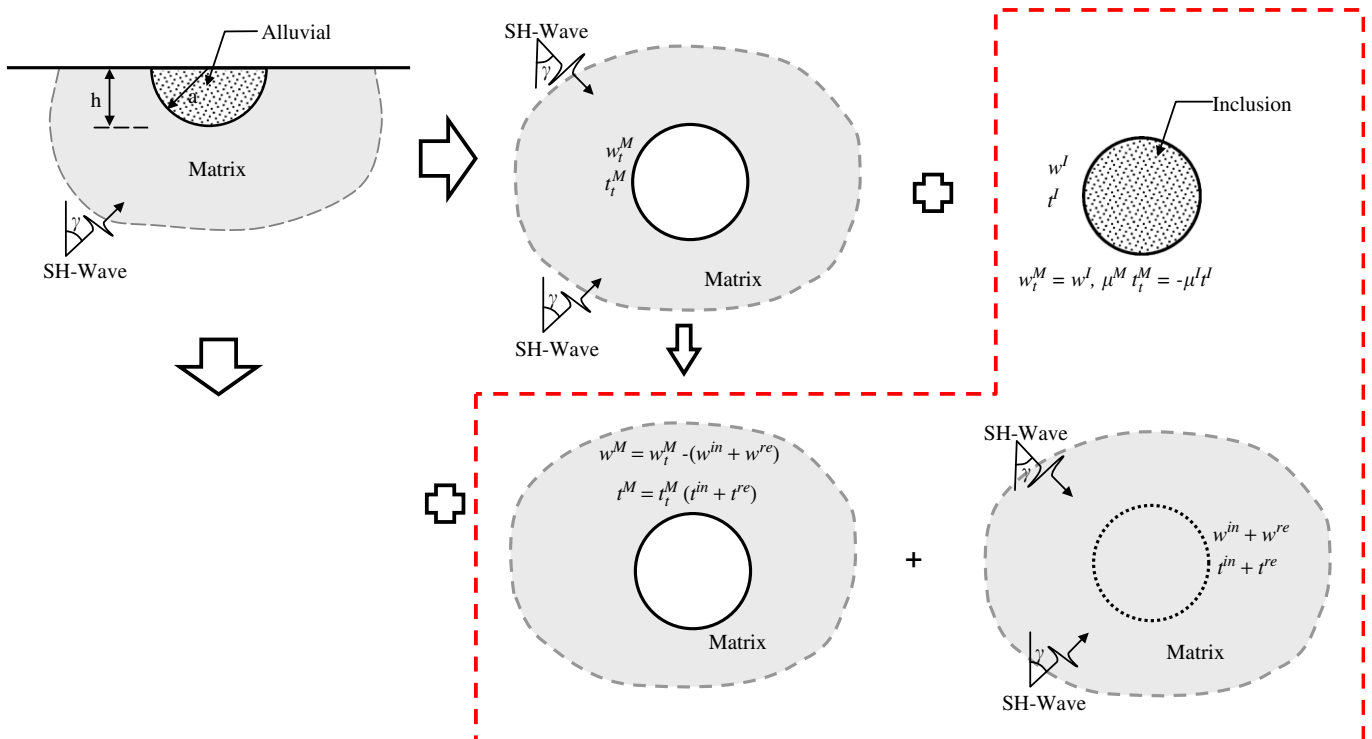


Fig. 4. Image concept and the decomposition of superposition of an alluvial valley.

$$\{\mathbf{u}\} = \begin{Bmatrix} \mathbf{u}_1 \\ \mathbf{u}_2 \\ \mathbf{u}_3 \\ \vdots \\ \mathbf{u}_N \end{Bmatrix}, \quad \{\mathbf{t}\} = \begin{Bmatrix} \mathbf{t}_1 \\ \mathbf{t}_2 \\ \mathbf{t}_3 \\ \vdots \\ \mathbf{t}_N \end{Bmatrix}, \quad (27)$$

where the vectors $\{\mathbf{u}\}$ and $\{\mathbf{t}\}$ are the Fourier coefficients and the first subindex “ j ” ($j = 1, 2, \dots, N$) in $[\mathbf{U}_{jk}]$ and $[\mathbf{T}_{jk}]$ denotes the j th circle where the collocation point is located and the second subindex “ k ” ($k = 1, 2, \dots, N$) denotes the k th circle with boundary data $\{\mathbf{u}_k\}$ and $\{\mathbf{t}_k\}$. The coefficient matrix of the linear algebraic system is partitioned into blocks, and each off-diagonal block corresponds to the influence matrices between two different circular boundaries. The diagonal blocks are the influence matrices due to themselves in each individual circle. After uniformly collocating $2L + 1$ points along the k th circular boundary, the submatrix can be written as

$$[\mathbf{U}_{jk}] = \begin{bmatrix} U_{jk}^{0c}(\phi_1) & U_{jk}^{1c}(\phi_1) & U_{jk}^{1s}(\phi_1) & \cdots & U_{jk}^{Lc}(\phi_1) & U_{jk}^{Ls}(\phi_1) \\ U_{jk}^{0c}(\phi_2) & U_{jk}^{1c}(\phi_2) & U_{jk}^{1s}(\phi_2) & \cdots & U_{jk}^{Lc}(\phi_2) & U_{jk}^{Ls}(\phi_2) \\ U_{jk}^{0c}(\phi_3) & U_{jk}^{1c}(\phi_3) & U_{jk}^{1s}(\phi_3) & \cdots & U_{jk}^{Lc}(\phi_3) & U_{jk}^{Ls}(\phi_3) \\ \vdots & \vdots & \vdots & \ddots & \vdots & \vdots \\ U_{jk}^{0c}(\phi_{2L}) & U_{jk}^{1c}(\phi_{2L}) & U_{jk}^{1s}(\phi_{2L}) & \cdots & U_{jk}^{Lc}(\phi_{2L}) & U_{jk}^{Ls}(\phi_{2L}) \\ U_{jk}^{0c}(\phi_{2L+1}) & U_{jk}^{1c}(\phi_{2L+1}) & U_{jk}^{1s}(\phi_{2L+1}) & \cdots & U_{jk}^{Lc}(\phi_{2L+1}) & U_{jk}^{Ls}(\phi_{2L+1}) \end{bmatrix}, \quad (28)$$

$$[\mathbf{T}_{jk}] = \begin{bmatrix} T_{jk}^{0c}(\phi_1) & T_{jk}^{1c}(\phi_1) & T_{jk}^{1s}(\phi_1) & \cdots & T_{jk}^{Lc}(\phi_1) & T_{jk}^{Ls}(\phi_1) \\ T_{jk}^{0c}(\phi_2) & T_{jk}^{1c}(\phi_2) & T_{jk}^{1s}(\phi_2) & \cdots & T_{jk}^{Lc}(\phi_2) & T_{jk}^{Ls}(\phi_2) \\ T_{jk}^{0c}(\phi_3) & T_{jk}^{1c}(\phi_3) & T_{jk}^{1s}(\phi_3) & \cdots & T_{jk}^{Lc}(\phi_3) & T_{jk}^{Ls}(\phi_3) \\ \vdots & \vdots & \vdots & \ddots & \vdots & \vdots \\ T_{jk}^{0c}(\phi_{2L}) & T_{jk}^{1c}(\phi_{2L}) & T_{jk}^{1s}(\phi_{2L}) & \cdots & T_{jk}^{Lc}(\phi_{2L}) & T_{jk}^{Ls}(\phi_{2L}) \\ T_{jk}^{0c}(\phi_{2L+1}) & T_{jk}^{1c}(\phi_{2L+1}) & T_{jk}^{1s}(\phi_{2L+1}) & \cdots & T_{jk}^{Lc}(\phi_{2L+1}) & T_{jk}^{Ls}(\phi_{2L+1}) \end{bmatrix}, \quad (29)$$

where ϕ_j , $j = 1, 2, \dots, 2L + 1$, are the angles of collocation along the circular boundary. Although both the matrices in Eqs. (28) and (29) are not sparse, it is found that the higher order harmonics is considered, the lower influence coefficients in numerical experiments is obtained. It is noted that the superscript “0s” in Eqs. (28) and (29) disappears since $\sin(0 \cdot \theta) = 0$. The elements of $[\mathbf{u}_{jk}]$ and $[\mathbf{T}_{jk}]$ are defined respectively as

$$U_{jk}^{nc}(\phi_m) = \int_{B_k} U(s_k, x_m) \cos(n\theta_k) R_k d\theta_k, \\ n = 0, 1, 2, \dots, L, \quad m = 1, 2, \dots, 2L + 1, \quad (30)$$

$$U_{jk}^{ns}(\phi_m) = \int_{B_k} U(s_k, x_m) \sin(n\theta_k) R_k d\theta_k, \\ n = 0, 1, 2, \dots, L, \quad m = 1, 2, \dots, 2L + 1, \quad (31)$$

$$T_{jk}^{ns}(\phi_m) = \int_{B_k} T(s_k, x_m) \cos(n\theta_k) R_k d\theta_k, \\ n = 0, 1, 2, \dots, L, \quad m = 1, 2, \dots, 2L + 1, \quad (32)$$

$$T_{jk}^{nc}(\phi_m) = \int_{B_k} T(s_k, x_m) \sin(n\theta_k) R_k d\theta_k, \\ n = 0, 1, 2, \dots, L, \quad m = 1, 2, \dots, 2L + 1, \quad (33)$$

where k is no sum, $k = (R_k, \theta_k)$, and ϕ_m is the polar angle of the collocation point x_m . The physical meaning of influence coefficients in Eqs. (30)–(33) denotes the response at ϕ_m on the j th circles due to singularity distribution of $\cos(n\theta)$ or $\sin(n\theta)$ on the k th circle as shown in Fig. 3. Chen [24] has provided the analytical evaluations of the integrals for each element in the influence matrix which are all non-singular. From the limiting process, the continuous and jump behavior across the boundary is also described. The direction of contour integration should be taken care, i.e.

counterclockwise and clockwise directions are for the interior and exterior problems, respectively. By rearranging the known and unknown sets, the Fourier coefficients can be obtained.

7. Image technique for solving half-plane scattering problems

7.1. Image concept for half-plane problems

For the half-plane problem with an alluvial valleys as shown in Fig. 4, we extend the problem into a full plane with the scatter by using the image concept such that our formulation can be applied. By applying the concept of even function, the symmetry condition is utilized to satisfy the traction free ($t = 0$) condition on the ground surface.

We merge the half-plane domain into the full-plane problem by adding with the reflective wave. To solve the problem, the decomposition technique is employed by introducing two plane waves, one is incident and the other is reflective, instead of only one incident wave. After taking the free body of full-plane problem through the ground surface, we obtain the desired solution which satisfies the Helmholtz equation and all the boundary conditions in the half-plane domain.

7.2. Decomposition of scattering problem into incident wave field and radiation problems

For the scattering problem subject to the incident wave, this problem can be decomposed into two parts. One is

the incident wave field and another is the radiation field as shown in Fig. 4. The relations between two parts are shown as

$$u_t^M = u^{in} + u^{re} + u^M, \tag{34}$$

$$t_t^M = t^{in} + t^{re} + t^M, \tag{35}$$

where the “ t_t^M ” denotes the total field of matrix including radiation and scattering. The subscripts “in” and “re” are the incident and reflected waves and the “ t^M ” denotes the radiation part of matrix and needs to be solved. To match the boundary condition for the cavity case, the total traction is defined as $t_t^M = 0$. For the inclusion case, we have the two constraints of the continuity of displacement and equilibrium of traction along the

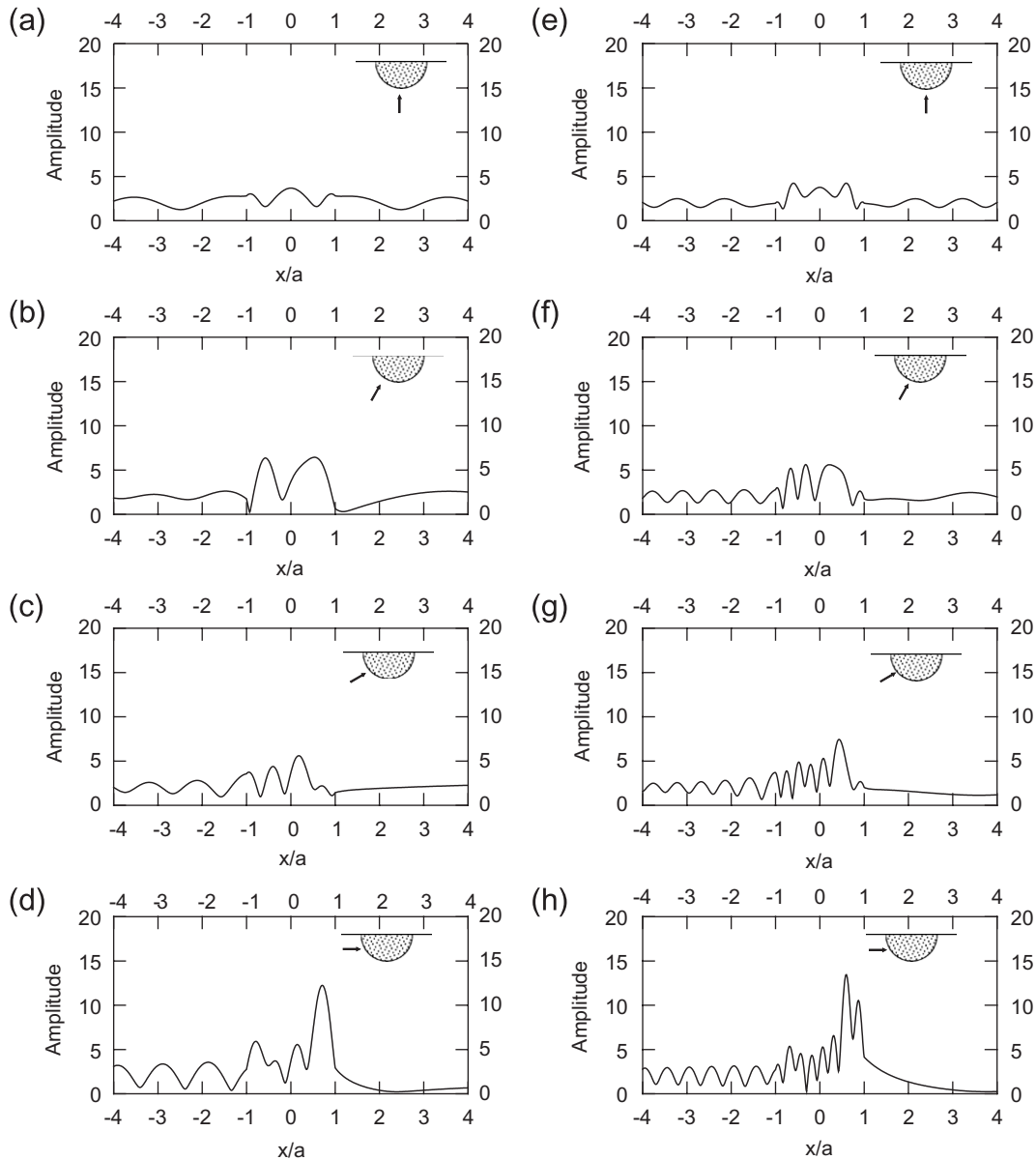


Fig. 5. Surface amplitudes of the alluvial valley problem for $\mu^I/\mu^M = \frac{1}{6}$ and $\rho^I/\rho^M = \frac{2}{3}$. (a)–(d) $\eta = 1.0$; (e)–(h) $\eta = 2.0$. (a) $\gamma = 0^\circ$, (b) $\gamma = 30^\circ$, (c) $\gamma = 60^\circ$, (d) $\gamma = 90^\circ$, (e) $\gamma = 0^\circ$, (f) $\gamma = 30^\circ$, (g) $\gamma = 60^\circ$, (h) $\gamma = 90^\circ$.

k th interface ($B_k, k = 1, \dots, N$) as

$$u_t^M = u^I \quad \text{on } B_k, \tag{36}$$

$$\mu^M t_t^M = -\mu^I t^I \quad \text{on } B_k. \tag{37}$$

The radiation parts of matrix (u^M and t^M) and inclusion (u^I and t^I) can be solved by employing our method.

8. Matching of interface conditions for problems of inclusion

According to the linear algebraic system, the two systems of matrix and inclusion yield

$$[U^M]\{t^M\} = [T^M]\{u^M\}, \tag{38}$$

$$[U]\{t^I\} = [T^I]\{u^I\}. \tag{39}$$

By employing the image concept and the decomposition of superposition, Eq. (38) can be rewritten as

$$[U^M]\{t_t^M - t^{in+re}\} = [T^M]\{u_t^M - u^{in+re}\}. \tag{40}$$

According to Fig. 4, an alluvial valley problem can be extended to a full-plane problem with a circular inclusion. In order to satisfy the traction free condition on the surface, the reflective wave is chosen to satisfy the symmetry condition as

$$w^{re} = W_0 e^{ik(x \sin \gamma - y \cos \gamma)}, \tag{41}$$

and we have the two constraints of the continuity of displacement and equilibrium of traction along the j th

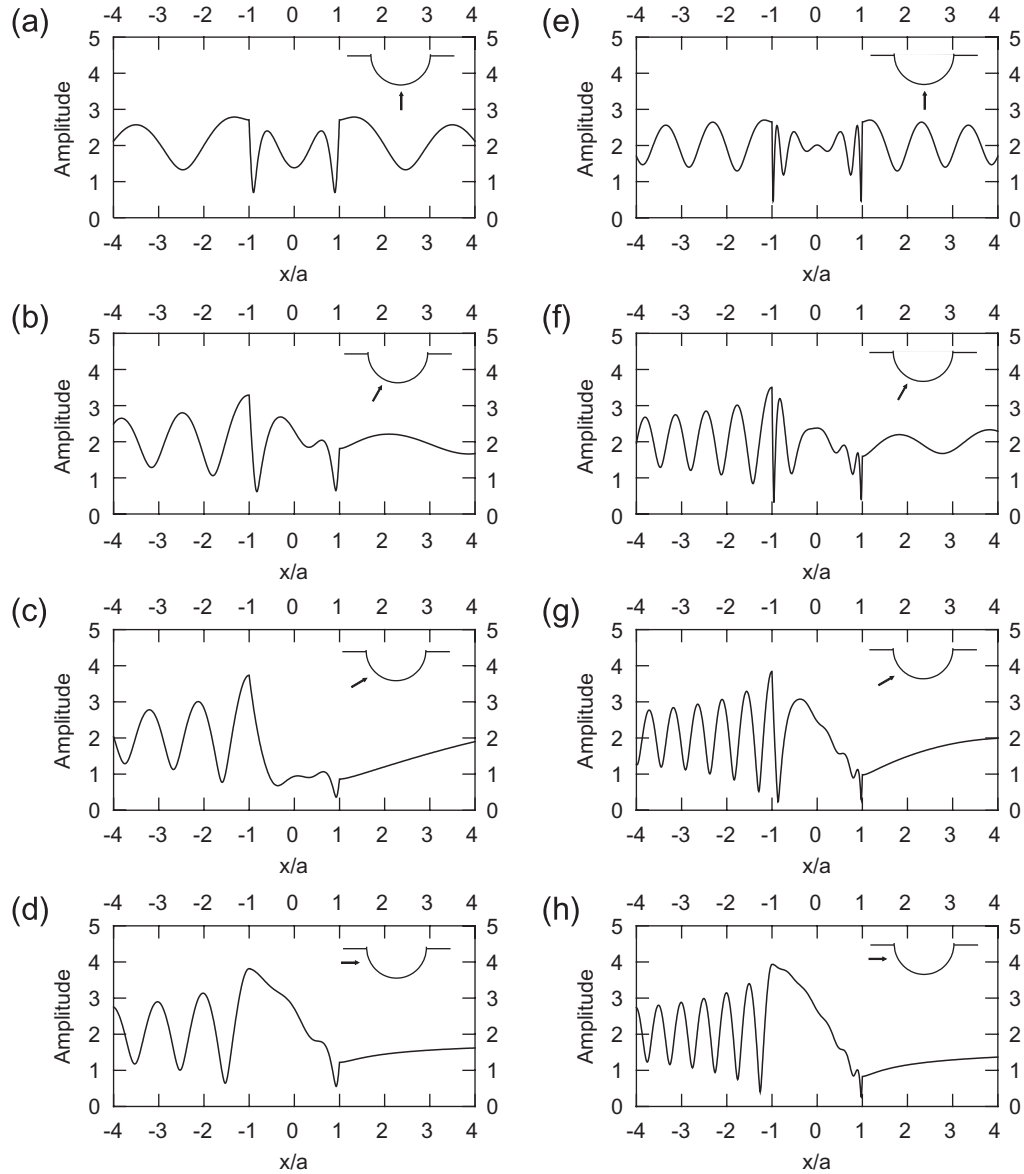


Fig. 6. Limiting case of a canyon ($\mu^I/\mu^M = 10^{-8}$ and $\rho^I/\rho^M = \frac{2}{3}$). (a)–(d) $\eta = 1$; (e)–(h) $\eta = 2$. (a) $\gamma = 0^\circ$, (b) $\gamma = 30^\circ$, (c) $\gamma = 60^\circ$, (d) $\gamma = 90^\circ$, (e) $\gamma = 0^\circ$, (f) $\gamma = 30^\circ$, (g) $\gamma = 60^\circ$, (h) $\gamma = 90^\circ$.

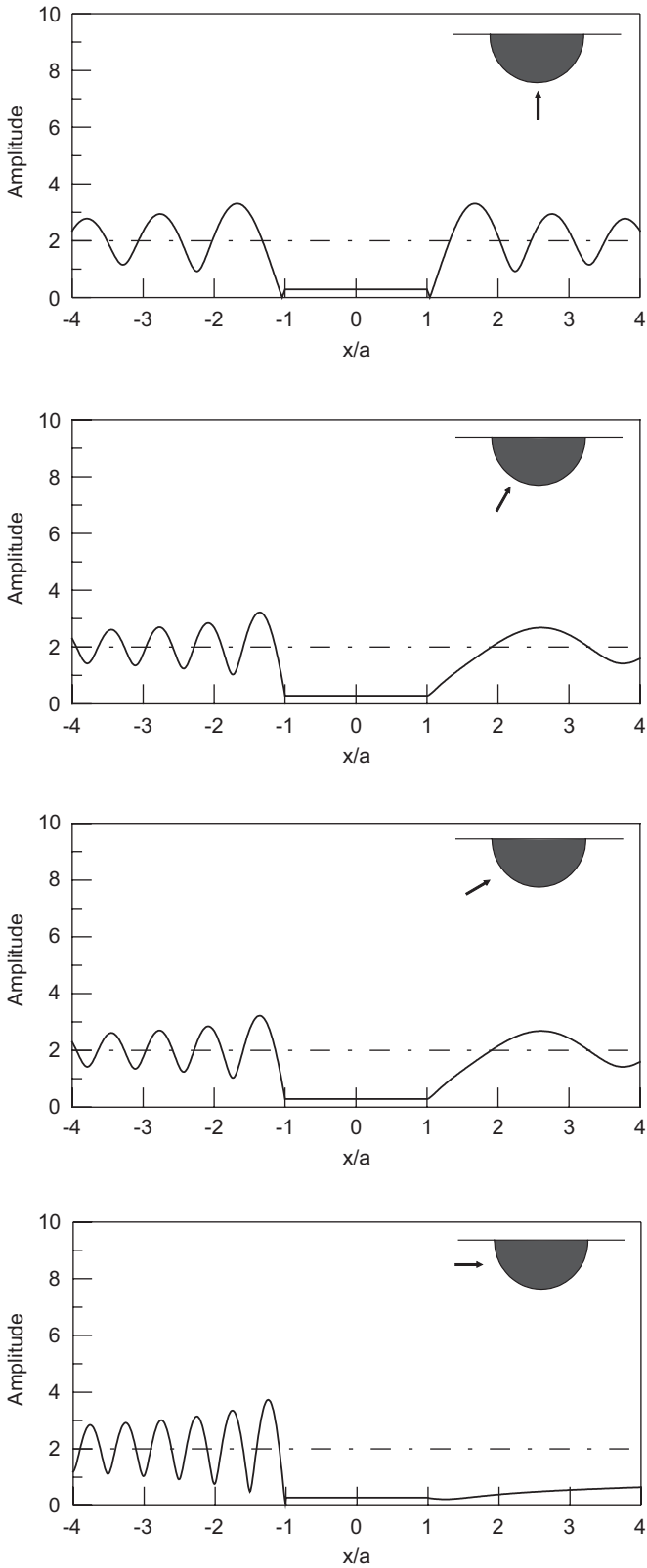


Fig. 7. Limiting case of a rigid alluvial valley ($\mu^I = /\mu^M = 10^4$, $\rho^I/\rho^M = \frac{2}{3}$ and $\eta = 2$). $\mu = 0^\circ$, $\gamma = 30^\circ$, $\gamma = 60^\circ$, $\gamma = 90^\circ$.

interface (B_j). We will employ the two constrains into the formulation as

$$\{\mathbf{u}_t^M\} = \{\mathbf{u}_t^I\} \quad \text{on } B_k, \quad (42)$$

$$[\boldsymbol{\mu}^M]\{\mathbf{t}_t^M\} = -[\boldsymbol{\mu}^I]\{\mathbf{t}_t^I\} \quad \text{on } B_k, \quad (43)$$

where $[\boldsymbol{\mu}^M]$ and $[\boldsymbol{\mu}^I]$ can be defined as follows:

$$[\boldsymbol{\mu}^M] = \begin{bmatrix} \mu^M & 0 & \dots & 0 \\ 0 & \mu^M & \dots & 0 \\ \vdots & \vdots & \ddots & \vdots \\ 0 & 0 & \dots & \mu^M \end{bmatrix}, \quad (44)$$

$$[\boldsymbol{\mu}^I] = \begin{bmatrix} \mu^I & 0 & \dots & 0 \\ 0 & \mu^I & \dots & 0 \\ \vdots & \vdots & \ddots & \vdots \\ 0 & 0 & \dots & \mu^I \end{bmatrix},$$

where μ^M and μ^I denote the shear modulus of the matrix and the k th inclusion, respectively. By assembling the matrices in Eqs. (39), (40), (42) and (43), we have

$$\begin{bmatrix} \mathbf{T}^M & -\mathbf{U}^M & \mathbf{0} & \mathbf{0} \\ \mathbf{0} & \mathbf{0} & \mathbf{T}^I & -\mathbf{U}^I \\ \mathbf{I} & \mathbf{0} & -\mathbf{I} & \mathbf{0} \\ \mathbf{0} & \boldsymbol{\mu}^M & \mathbf{0} & \boldsymbol{\mu}^I \end{bmatrix} \begin{Bmatrix} \mathbf{u}_t^M \\ \mathbf{t}_t^M \\ \mathbf{u}_t^I \\ \mathbf{t}_t^I \end{Bmatrix} = \begin{Bmatrix} \mathbf{u}(\mathbf{x})^{\text{in+re}} \\ \mathbf{0} \\ \mathbf{0} \\ \mathbf{0} \end{Bmatrix}, \quad (45)$$

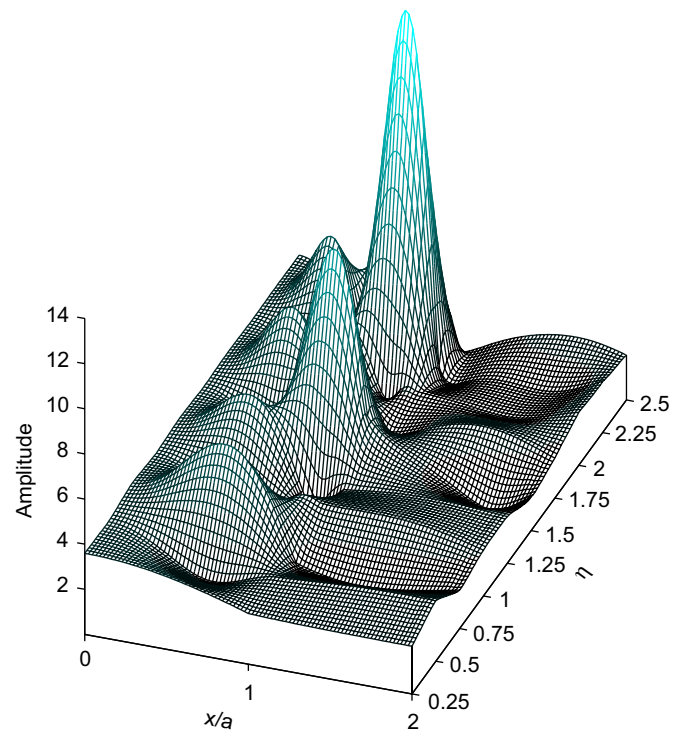


Fig. 8. Surface displacements as a function of x/a and η for the vertical incidence ($\gamma = 0^\circ$, $\rho^I/\rho^M = \frac{2}{3}$ and $c^I/c^M = \frac{1}{3}$).

where $[\mathbf{I}]$ is the identity matrix, and $\{\mathbf{u}(\mathbf{x})^{\text{in+re}}\}$ as

$$\{\mathbf{u}(\mathbf{x})^{\text{in+re}}\} = \langle \mathbf{T}^M \quad -\mathbf{U}^M \rangle \left\{ \begin{matrix} \mathbf{u}^{\text{in}} + \mathbf{u}^{\text{re}} \\ \mathbf{t}^{\text{in}} + \mathbf{t}^{\text{re}} \end{matrix} \right\}. \quad (46)$$

After obtaining the unknown Fourier coefficients, the origin of observer system is set to c_j in the B_j integration as shown in Fig. 2(b) to obtain the potential by employing Eq. (6). For the problem of multiple scatters (N alluvial valleys), the dimension of influence matrices becomes $N \times [4 \times (2L + 1)]$ by $N \times [4 \times (2L + 1)]$. In the recent investigation, we have extended to the four inclusions problem in our thesis [24].

In order to check the validity of the formulation, the Manoogian [6] and Trifunac's [1] problem with an alluvial valley is revisited. We follow the same parameter, η , for comparison purpose. The dimensionless frequency η is

defined as

$$\eta = \frac{2a}{\lambda} = \frac{k^M a}{\pi} = \frac{\omega a}{\pi c^M}, \quad (47)$$

where a is the half-width of the alluvial valley, ω is the angular frequency, k^M and c^M are the shear wave number and the velocity of shear wave for the matrix medium, and the shear wave number k is defined as

$$k = \frac{\omega}{c}. \quad (48)$$

Substituting Eq. (47) into Eq. (48), the wave number of matrix field is rewritten as

$$k^M = \frac{\pi \eta}{a}, \quad (49)$$

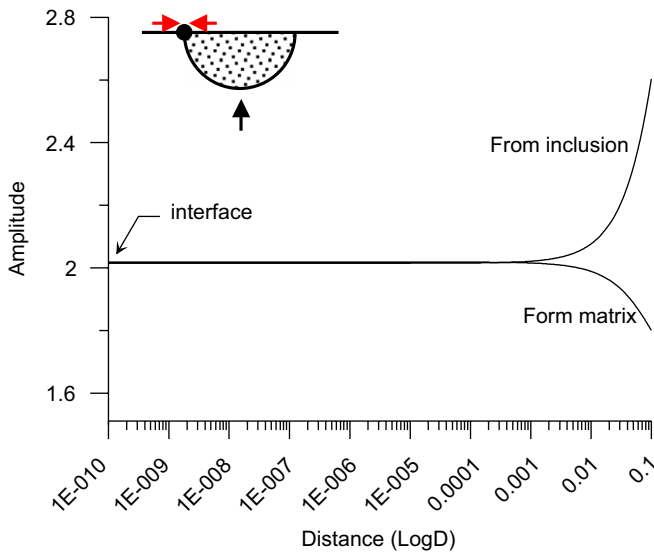


Fig. 9. Amplitudes of the points near the corner for the interface boundary.

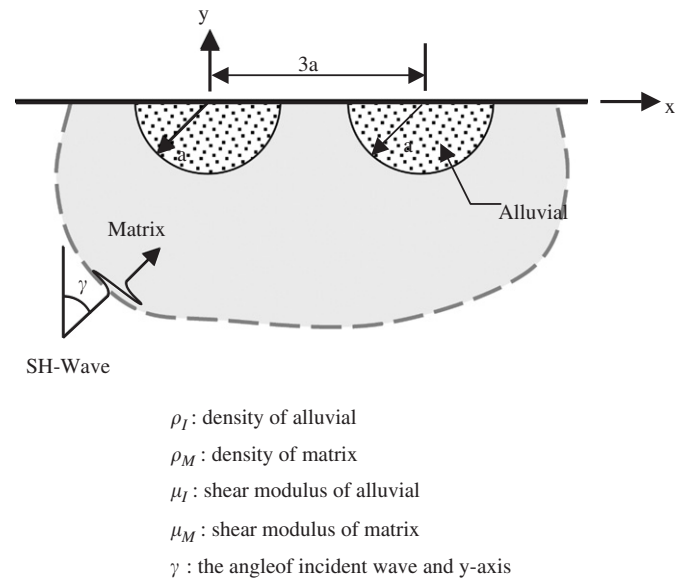


Fig. 11. A half-plane problem with two alluvial valleys subject to the incident SH-wave.

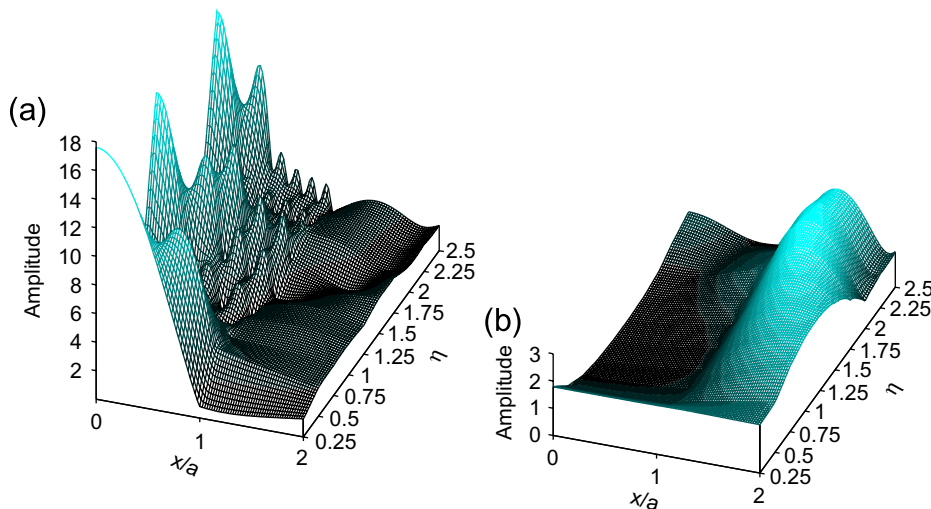


Fig. 10. Spectral displacement with harder material of alluvial valley versus the dimensionless frequency η for the vertically incident SH-wave. (a) $\rho_I/\rho_M = 2/3$ and $c^I/c^M = 1/3$, (b) $\rho_I/\rho_M = 3/2$ and $c^I/c^M = 2$.

and the shear wave number for the inclusion field is obtained by

$$\frac{k^I}{k^M} = \frac{c^E}{c^I} = \left(\frac{\mu^M}{\mu^I} \cdot \frac{\rho^I}{\rho^M} \right)^{1/2} \quad (50)$$

Eq. (50) indicates that various mediums yield different wave numbers. The surface amplitude is an important index for the earthquake engineering. If the amplitude of incident plane SH-wave is one, the responses at different locations represent amplifications of the incident wave. The resultant motion is defined by the modulus

$$\text{Amplitude} = \sqrt{\text{Re}^2(w) + \text{Im}^2(w)}, \quad (51)$$

where $\text{Re}(w)$ and $\text{Im}(w)$ are the real and imaginary parts of total displacement, respectively.

9. Illustrative examples and discussions

In the section, we revisit the same problems of Manoogian and Lee [7], Trifunac [1] and Tsaur et al. [25] for the alluvial problem. In order to check the accuracy of the present method, the limiting case is conducted. All the numerical results are given below by using 10 terms of Fourier series.

Case 1: Half-plane problem with an alluvial valley subject to the SH-wave.

In the following examples, we choose the same parameters, $\mu^I/\mu^M = \frac{1}{6}$ and $\rho^I/\rho^M = \frac{2}{3}$ which were previously adopted in the Ph.D. dissertation of Manoogian [6]. Fig. 5 shows the surface amplitudes for the parameters of $\eta = 1$

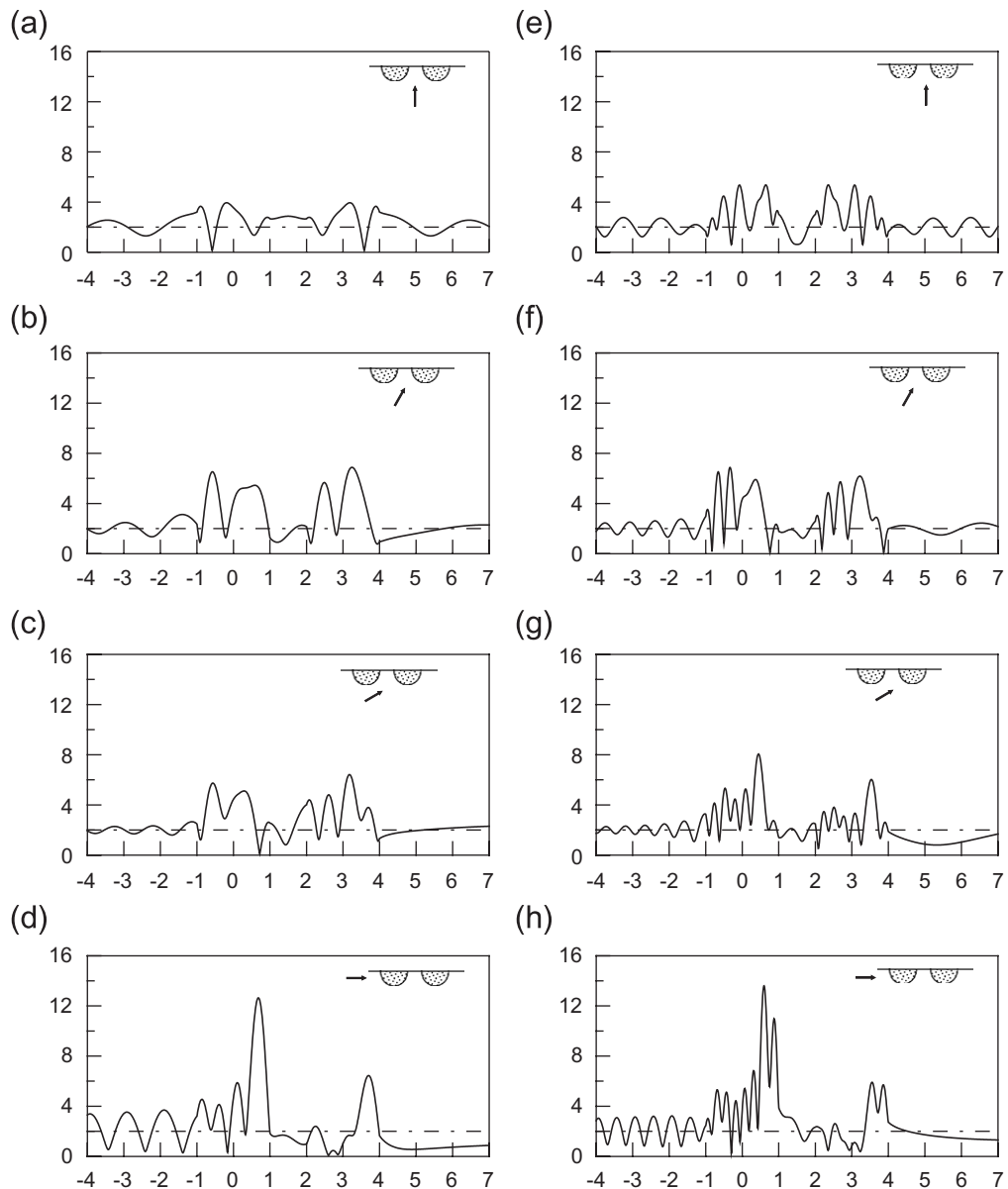


Fig. 12. Surface displacements of two alluvial valleys ($\mu^I/\mu^M = \frac{1}{6}$ and $\rho^I/\rho^M = \frac{2}{3}$). (a)–(d) $\eta = 1.0$; (e)–(h) $\eta = 2.0$. (a) $\gamma = 0^\circ$, (b) $\gamma = 30^\circ$, (c) $\gamma = 60^\circ$, (d) $\gamma = 90^\circ$, (e) $\gamma = 0^\circ$, (f) $\gamma = 30^\circ$, (g) $\gamma = 60^\circ$, (h) $\gamma = 90^\circ$.

and 2. For two states of η , four various incident angles ($\gamma = 0^\circ, 30^\circ, 60^\circ$ and 90°) are considered. The figures show the displacement amplitude on the ground surface only. Displacements are plotted with respect to the dimensionless distance x/a for a specified parameter η . In order to verify the limiting case of the general program, we set $\mu^I/\mu^M = 10^{-8}$ to reduce to two canyon cases of η (1.0 and 2.0). In Fig. 6, good agreements are obtained after comparing with Lee and Manooogian's results [26] for various frequency parameters of η for the semi-circular canyon case. Others are shown in the master thesis [24]. Another limiting case of the rigid alluvial is also of interest in the foundation engineering. For example, rigid footing

is a popular model in geotechnical engineering. By setting μ^I/μ^M to be infinity, the limiting case of rigid inclusion can be obtained. Fig. 7 plots the surface displacement by setting $\mu^I/\mu^M = 10^4$ and $\eta = 2$ in the real computation. In the range of $x/a = -1$ to 1, the amplification is a constant as expected, because it is undeformed due to the rigid alluvial.

Figs. 8 and 10 show the surface displacement for $\eta = 0.25, \dots, 2.25$ and 2.50 , for various values of ρ^I/ρ^M and c^I/c^M , subject to the vertically incident SH-wave ($\gamma = 0^\circ$) whose amplitude is one. The point $x/a = 1$ corresponds to the edge of the alluvial valley, and the position of $x/a = 0$, shows the center of alluvial valley. Since all displacement amplitudes are symmetric about the

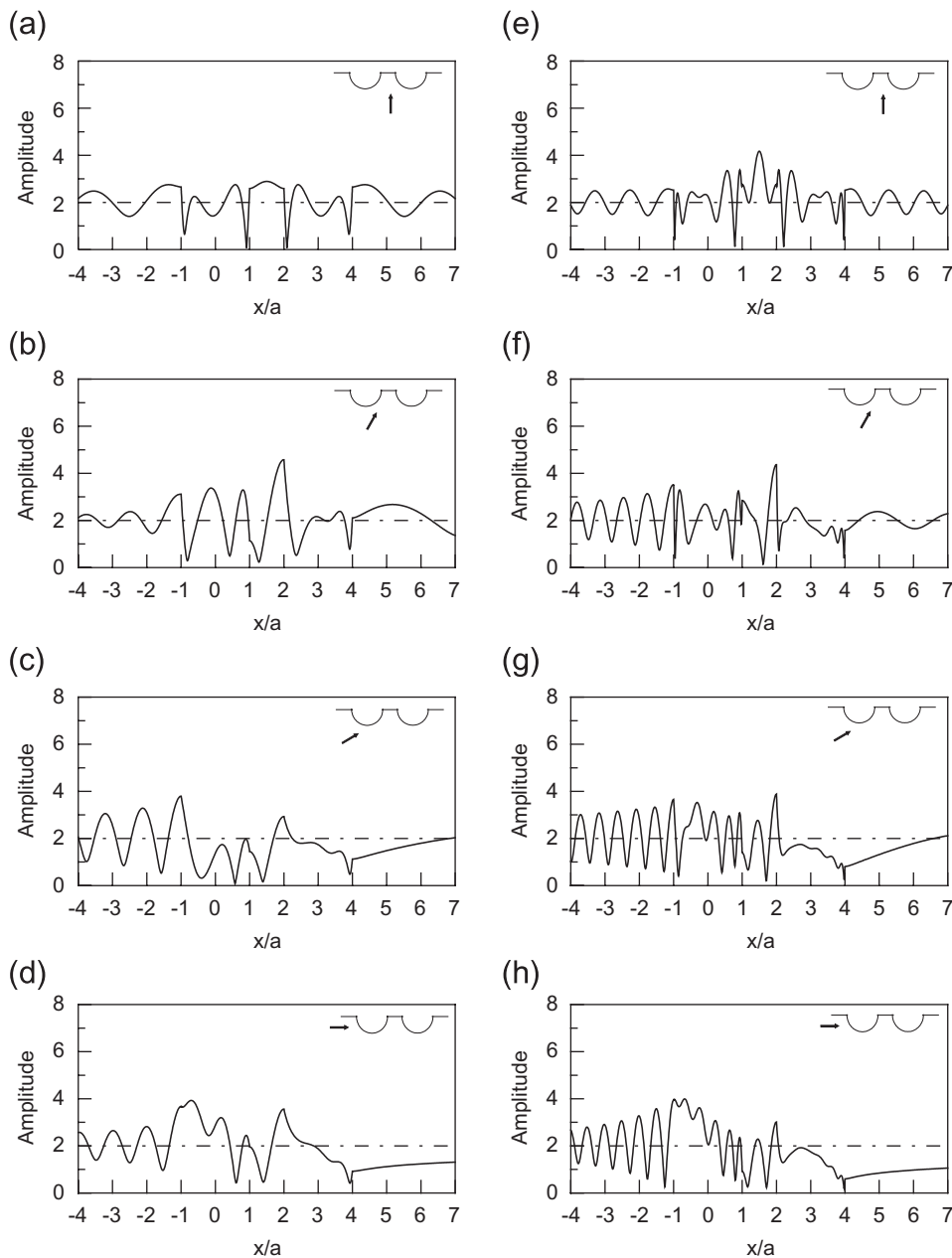


Fig. 13. Limiting case of two canyons ($\mu^I/\mu^M = 10^{-8}$ and $\rho^I/\rho^M = \frac{2}{3}$). (a)–(d) $\eta = 1$; (e)–(h) $\eta = 2$. (a) $\gamma = 0^\circ$, (b) $\gamma = 30^\circ$, (c) $\gamma = 60^\circ$, (d) $\gamma = 90^\circ$, (e) $\gamma = 0^\circ$, (f) $\gamma = 30^\circ$, (g) $\gamma = 60^\circ$, (h) $\gamma = 90^\circ$.

center, for the vertically incident SH-wave, only the positive x/a -axis is illustrated. In Figs. 8 and 10, they show the effect of c^I/c^M on the surface amplitudes. The soft-basin effect of high amplitude is observed in this study. Fig. 10(b) is an example of harder material in the alluvial valley and softer matrix. It is found that the surface amplitude is two as expected when η is small. For the far field response, the surface amplitude is found to be two since the perturbation due to the alluvial/inclusion is small. All of the figures have good agreement after comparing with Trifunac's [1] results. Amplitudes of the points near the corner for the interface boundary are shown as Fig. 9 and no boundary-layer effect of the present method is found Fig. 10.

Case 2: Half-plane problem with two alluvial valleys subject to the SH-wave.

Two semi-circular alluvial valleys subject to the incident SH-wave of γ angle are shown in Fig. 11. Fig. 12 shows the surface displacements versus x/a for various incident angles with $\mu^I/\mu^M = \frac{1}{6}$ and $\rho^I/\rho^M = \frac{2}{3}$ subject to two cases of η (1.0 and 2.0). By setting $\mu^I/\mu^M = 10^{-8}$, the limiting case of successive canyons is obtained as shown in Fig. 13. Tsaour et al. [25] and Fang [27] have both calculated the problem of two semi-circular alluvial valleys for the incident SH-wave. Tsaour et al. [25] pointed out that the deviation by Fang [27] is that Fang improperly used the orthogonal property. Good agreement is made after comparing with the results of Tsaour et al. [25]. In the literature, we can find the case of successive alluvial valleys to compare with our data, but we have high confidence of our results according to previous experiences. For the incident angle of zero-degree, the surface displacement amplitude is symmetric. By increasing the incident angle, the displacement amplitude is gradually smaller in the back side of the alluvial valley or canyon due to the shield effect of two alluvial valleys or canyons. As the incident angle approaches 90° , the surface displacement amplitudes are all smaller than the "free field" in the back of the second alluvial. It indicates that two alluvial valleys can be the wave trap for the incident wave.

10. Conclusions

The first attempt to employ degenerate kernel in BIEM for problems with circular boundaries subject to the SH-wave was achieved. Not only canyon but also alluvial valley problems were treated. We have proposed a BIEM formulation by using degenerate kernels, null-field integral equation and Fourier series in companion with adaptive observer systems and vector decomposition. This method is a semi-analytical approach for problems with circular boundaries since only truncation error in the Fourier series is involved. Two limiting cases of inclusions, canyon and rigid footing, was also addressed. Good agreements are obtained after comparing with previous results. The surface motion of half-plane problem with alluvial valleys was determined. Parameter study on the surface amplitudes

was also addressed. The analysis of amplification and interference effects for valley and inclusions subject to SH-waves may explain the ground motion either observed or recorded during earthquake. The method shows great generality and versatility for the problems with multiple circular cavities and inclusions of arbitrary radii and positions. Five advantages of singularity-free, no boundary-layer effect, well-posed model, exponential convergence and mesh-free approach are the main features of the proposed approach.

References

- [1] Trifunac MD. Surface motion of a semi-cylindrical alluvial valley for incident plane SH waves. *Bull Seismol Soc Am* 1971;61(6):1755–70.
- [2] Pao YH, Mow CC. 1972, Diffraction of elastic waves and dynamics stress concentration. Crane, New York.
- [3] Trifunac MD. Scattering of plane SH waves by a semi-cylindrical canyon. *Earthquake Eng Struct Dyn* 1973;1:267–81.
- [4] Lee VW, Trifunac MD, ASCE AM. Response of tunnels to incident SH-waves. *J Eng Mech Div* 1978;105(EM4):643–59.
- [5] Lee VW, Manoogian ME. Surface motion above an arbitrary shape underground cavity for incident SH waves. *Eur Earthquake Eng* 1995;1:3–11.
- [6] Manoogian ME. 1992, Scattering and difference of plane SH-waves by surface and subsurface discontinuities. PhD dissertation, Department of Civil Engineering of University, Southern California, USA.
- [7] Manoogian ME, Lee VW. Diffraction of SH-waves by subsurface inclusions of arbitrary shape. *J Eng Mech* 1996;122(2):123–9.
- [8] Rodríguez-Castellanos A, Luzon F, Sánchez-Sesma FJ. Diffraction of seismic waves in an elastic, cracked half plane using boundary integral formulation. *Soil Dyn Earthquake Eng* 2005;25:827–37.
- [9] Bielak J, MacCamy RC, McGhee DS, Barry A. Unified Symmetric BEM-FEM for site effects on ground motion—SH wave. *J Eng Mech* 1991;117(10):2265–85.
- [10] Kawase H. Time-domain response of a semi-circular canyon for incident SV, P and Rayleigh waves calculated by the discrete wavenumber boundary element method. *Bull Seismol Soc Am* 1988; 74(4):1415–37.
- [11] Kawase H, Sato T, Sate S, Tanaka G. Analytical and observational study on seismic scattering problem of a site with geological irregularity. In: *Transactions of the International Conference on Structural Mechanics in Reactor Technology*, vol. K, 1985.
- [12] Gil-Zepeda SA, Montalvo-Arrieta JC, Vai R, Sánchez-Sesma FJ. A hybrid indirect boundary element-discrete wave number method applied to simulate the seismic response of stratified alluvial valleys. *Soil Dyn Earthquake Eng* 2003;23:77–86.
- [13] Rodríguez-Castellanos A, Sánchez-Sesma FJ, Luzon F, Martín R. Multiple scattering of elastic waves by subsurface fractures and cavities. *Bull Seismol Soc Am* 2006;96(4):1359–74.
- [14] Guiggiani M. Hypersingular boundary integral equations have an additional free term. *Comput Mech* 1995;16:245–8.
- [15] Gray LJ, Manne LL. Hypersingular integrals at a corner. *Eng Anal Boundary Elem* 1993;11:327–34.
- [16] Watermann PC. Matrix formulation of electromagnetic scattering. *Proc IEEE* 1965;53:805–12.
- [17] Doicu A, Wriedt T. Extended boundary condition method with multiple sources located in the complex plane. *Opt Commun* 1997; 139:85–91.
- [18] Achenbach JD, Kechter GE, Xu Y-L. Off-boundary approach to the boundary element method. *Comput Methods Appl Mech Eng* 1988; 70:191–201.
- [19] Kress R. *Linear Integral equations*. Berlin: Springer-Verlag; 1989.
- [20] Atkinson KE. *The numerical solution of integral equations of the second kind*. New York: Cambridge University Press; 1997.

- [21] Kress R. On the numerical solution of a hypersingular integral equation in scattering theory. *J Comput Appl Math* 1995;61: 345–60.
- [22] Chen JT, Hong H-K. Review of dual boundary element methods with emphasis on hypersingular integral and divergent series. *Appl Mech Rev* 1999;52:17–33.
- [23] Chen JT, Liu LW, Hong H-K. Spurious and true eigensolutions of Helmholtz BIEs and BEMs for a multiply connected problem. *Proc R Soc London Ser A* 2003;459:1891–924.
- [24] Chen PY. 2006, Null-field integral equation approach for solving stress concentration problems with circular boundaries. Master thesis, Department of Harbor and River Engineering, National Taiwan Ocean University, Taiwan.
- [25] Tsaur DH, Chang KH, Lin JG. Response of multiple semi-circular cylindrical canyons subjected to plane SH-wave. *Asia Pacific Rev Eng Sci Technol* 2004;2(2):251–66 (in Chinese).
- [26] Lee VW, Manoogian ME. Surface motion above an arbitrary shape underground cavity for incident SH waves. *Eur Earthquake Eng* 1995;1:3–11.
- [27] Fang YG. Scattering of plane SH-waves by multiple circular-arc valleys at the two-dimensional surface of the earth. *Earthquake Eng Eng Vib* 1995;15(1):85–91 (in Chinese).